Applied Catalysis B: Environmental 147 (2014) 49–57

Contents lists available at ScienceDirect

Applied Catalysis B: Environmental

journal homepage: www.elsevier.com/locate/apcatb

Fabrication and photocatalytic properties of cationic and anionic S-doped TiO_2 nanofibers by electrospinning

Dong Ma[a,b], Yanjun Xin[a,b], Mengchun Gao[a,*], Juan Wu[b]

[a] College of Environmental Science and Engineering, Ocean University of China, Qingdao, 266100, China
[b] College of Resource and Environment, Qingdao Agricultural University, Qingdao, 266109, China

ARTICLE INFO

Article history:
Received 1 February 2013
Received in revised form 31 July 2013
Accepted 6 August 2013
Available online 26 August 2013

Keywords:
Photocatalyst
TiO_2 nanofiber
Sulfur doped
Cationic and anionic doping
Electrospinning

ABSTRACT

In present work, S-doped TiO_2 nanofibers, with several hundred nanometers in diameter, have been prepared via electrospinning technique using thiourea and CS_2 as the sulfur precursors (denoted as UTF and CTF, respectively). The results revealed that sulfur atoms were successfully incorporated into the bulk phase of TiO_2 nanofibers. Cationic doping was found with the substitution of Ti^{4+} by S^{6+} and Ti—O—S bonds were formed in the UTF sample, but anionic doping was obtained in the CTF sample and O—Ti—S bonds were produced via the S^{2-} substituted for O^{2-}. Meanwhile, evidence showed that chemisorbed SO_4^{2-} groups were present on the surface of both S-doped samples. Furthermore, S-doping could effectively inhibit the growth of crystalline grain size and obviously increase light absorbance in visible region. The photocatalytic activity of obtained nanofibers was analyzed for the degradation of organic pollutants by visible-light irradiation, and the photocatalytic mechanism was investigated by employing several scavengers for active species. Results showed that photoinduced holes (h^+) and chemisorbed hydroxyls (OH_{ads}^-) on catalyst surface played a vital role in the photocatalysis of UTF system, but photoinduced holes (h^+) and electrons (e^-) had the nearly equal importance in CTF system.

1. Introduction

Electrospinning is a simple and low-priced technique for fabrication functional fibers, and various electrospun nanofibers have been successfully generated [1–3]. The obtained nanofibers have fibrous mat structure, large surface area and sufficient mechanical integrity, and are widely applied in many fields [4–7]. Among them, the preparation of TiO_2 nanofibers by electrospinning approach was first reported in 2003, based on polymer solgel solutions [8]. Subsequently, pure titania nanofibers were obtained successively via this convenient method, such as hollow fibers with mesoporous walls [9], nanofibers with large-linked particles [10], and single-crystalline rutile nanorods [11]. The fiber-type TiO_2 photocatalyst exhibits higher recyclable property than the powdery one because it is liable to be separated from water, and it surely will be a promising material for environmental purification.

However, one major limitation of TiO_2 photocatalyst is the negligible activity when irradiated with visible-light which occupies a large portion of solar light. To extend the response of TiO_2 nanofibers to the visible region, many studies have been carried out, such as noble metal deposition [12], semiconductors coupling [13], and ionic doping [14]. For example, Ag deposition TiO_2 [15] and SnO_2/TiO_2 bicomponent nanofibers [16] were prepared by electrospinning process and showing excellent photodegradation of MB and Rh B, respectively. Additionally, recent studies have shown that the desired band gap narrowing of TiO_2 nonafibers can also be achieved by using metal dopant, such as W [17], Er [18], La/Eu [19], Zr [20], or Fe [21]. The benefit of transition metal doping species is a red shift in the band gap transition or a visible-light absorption, which is attributed to the charge-transfer transition between the d electrons of the dopant and the conduction band (CB) or valence band (VB) of TiO_2 [22,23]. On the other hand, theoretical and experimental studies have shown that nonmetal dopant, such as nitrogen, introduces new states in the band gap close to the VB with both substitutional and interstitial impurities [24,25]. Modify TiO_2 nanofibers with N-doping via electrospinning method were reported by several groups [26–28]. The fabricated N-doped TiO_2 nanofibers or composite fibers brought about a narrowing in the band-gap and form a shifting of the absorption onset to the visible region.

S-doped TiO_2 has been studied extensively as well. S-doping induced a similar band gap narrowing as nitrogen [14], and the mixing of the sulfur 3p states with the VB was found to contribute to the increased width of the VB, leading to the narrowing of the band gap [29]. Recent studies showed that the ionic form of the S-doping is closely dependent on the preparation routes and sulfur sources. Umebayashi et al. [30] have succeeded in preparing S-doped TiO_2 nanoparticles using TiS_2 as precursor, and found that sulfur was

* Corresponding author. Tel.: +86 532 66781061; fax: +86 532 66781061.
E-mail address: mengchun@ouc.edu.cn (M. Gao).

0926-3373/$ – see front matter © 2013 Elsevier B.V. All rights reserved.
http://dx.doi.org/10.1016/j.apcatb.2013.08.004

doped as an anion and replaced the lattice oxygen in TiO_2. Later researches have shown parallel findings when taking TiS_2 or CS_2 as sulfur sources [31,32]. According to them, most of the sulfur in TiS_2 or CS_2 was oxidized and the residual sulfur would naturally remain as S^{2-}, and the sulfur modification further increased the V_P and the d_P since the O atom in the O—Ti—O network was replaced by the S atom. On the contrary, Ohno and other groups [33–36] found that sulfur atoms were incorporated as cations and replaced Ti ions when taking thiourea or sulfate as sulfur sources in the S-doped TiO_2 nanopowders. They confirmed that the substitution of Ti^{4+} by S^{6+} was chemically more favorable than replacing O^{2-} with S^{2-}, due to the different ionic radius among them. With the substitution of Ti^{4+} by S^{6+}, S 3s states induced states just above the O 2p valence states, and S 3p states contributed to the CB of TiO_2 [37]. Furthermore, other reports [38–40] announced that two ionic forms were present in the obtained TiO_2 nanoparticles with the sulfur precursor of thiourea.

Undeniably, S-doped TiO_2 photocatalyst continues to be a hot research topic. Nonetheless, to the best of our knowledge, there has been no report regarding the electrospun S-doped TiO_2 nanofibers, and it would be both scientifically and practically important. Herein, we developed a simple preparation method for the synthesis of S-doped TiO_2 nanofibers by electronspinning method. In the present work, thiourea and CS_2 were employed as the sulfur sources to enhance sulfur incorporation into TiO_2 lattice, and we focused on the sulfur ionic species with different sulfur precursors in electronspinning process. The visible-light responsive mechanism was discussed and the photocatalytic activity of the obtained nanofibers was evaluated using the degradation of Rhodamine B (Rh B) and phenol as a model reaction.

2. Experimental

2.1. Preparation of nanofibers

Titanium (IV) tetra-isopropoxide (TTIP, 97%), polyvinylpyrrolidone (PVP, MW 1,300,000), thiourea (TU, 99%) and carbon disulfide (CS_2, 99%) were obtained from Sigma-Aldrich. Acetic acid (CH_3COOH), ethanol (CH_3CH_2OH), sodium oxalate ($Na_2C_2O_4$), potassium dichromate [$K_2Cr_2O_7$ (Cr(VI)], and sodium fluoride (NaF) were analytical reagent and purchased from Aladdin Company, Shanghai, China. All chemicals were used without further purification.

The S-doped TiO_2 precursor sol was prepared by the following method. 1.0 g PVP was added into the 10 ml ethanol solution under vigorous stirring for about 30 min. A Ti precursor solution (prepared by mixing 5 mmol of TTIP, 5 mmol of TU or CS_2, 2 ml acetic acid and 5 ml ethanol) was then mixed with the above solution. After being aged for 2 h at room temperature, the spinnable sol was obtained.

In a typical electrospinning procedure, the spinnable sol was transferred into a glass injector, and was pressurized by a single channel micro-infusion pump (Longer pump LSP01-1A, Baoding, China). The injector was equipped with a 21 G metallic needle, which was connected to a high-voltage supply (DW-P303-1ACF0, Tianjin, China). A piece of stainless steel network (45 cm × 45 cm) was employed to collect the gel fibers. The distance between the needle and the target was 15 cm, and the applied voltage between them was 22 kV. The electrospinning process was carried out at room temperature. After stabilized in the air for 24 h, the as-spun fibers were then dried in vacuum oven at 60 °C for 12 h, and calcined at 500 °C for 2 h in air at a heating rate of 2 °C/min in order to remove organic matter completely. Finally, the obtained S-doped TiO_2 nanofibers with different sulfur dopants of thiourea and CS_2 were denoted as UTF and CTF, respectively. For comparison, the undoped TiO_2 nanofibers prepared by the same approach were denoted as TF.

2.2. Characteration

The microstructures of the TiO_2 photocatalyst were observed by a scanning electron microscope (SEM, JEOL 7500F, Japan) equipped with an energy dispersive X-ray (EDX) spectroscopy. The thermogravimetric (TG) curves were taken in a TA instrument (STD Q600), and the as-spun samples around 20 mg were heated in a static atmosphere of air, maintaining 10 °C/min heating rate from the ambient temperature to 800 °C. XRD patterns were tested on a *D*/max-A X-ray diffractometer (Rigaku, Japan) using Cu Kα radiation (λ = 0.1542 nm), and with the scanning speed of 10°/min in 2θ ranging from 10° to 80°. The accelerated voltage and applied current were 40 kV and 70 mA, respectively. The average crystallite sizes (D) of TiO_2 samples was calculated by applying the Debye-Scherrer equation, $D = 0.89\lambda/(B\cos\theta)$, where λ is the wavelength of the X-ray in nanometer, B is the width at half peak-height in radian, and θ is the angle between the incident and diffracted beams in degree. The content of anatase in TiO_2 samples and the unit cell parameters were calculated as previously reported methods [41,42]. X-ray photoelectron spectroscopy (XPS) were measured on an ESCALAB 250 spectrometer (Thermo Electron Corp, UK) with an Al Kα source and a charge neutralizer, and all spectra were calibrated to the C 1s peak at 284.6 eV. Fourier transform infrared (FT-IR) spectra were recorded in Avatar 370 spectrometer (Thermo Nicolet, USA). UV–vis diffuse reflectance spectra (DRS) were performed with a UV–vis spectrophotometer (TU 1901, China) with an integrating sphere attachment via $BaSO_4$ as background.

2.3. Photocatalytic activity

All experiments were carried out in an open fixed-bed photoreactor, equipped with a 500 W Xe lamp as visible-light source and a glass optical filter was inserted to cut off the short wave length components (λ < 420 nm). 0.25 g of photocatalyst was added to 250 ml of Rh B aqueous solution with an initial concentration of 15 mmol/l In order to exclude photosensitized effect in the photocatalytic process, the photocatalytic degradation of phenol (200 mmol/l) was also carried out by a same procedure. Before visible-light irradiation, the solution mixture was stirred for 30 min in dark to establish the adsorption/desorption equilibrium between the photocatalyst and Rh B (or phenol). The photocatalyst was separated from solution by filtration with a 0.45 μm syringe filter. The concentration of Rh B solution was measured with UV–vis spectrophotometer (TU1901, China) at 554 nm (phenol at 270 nm). To evaluate the photomineralization degree of target pollutants, the initial and final total organic carbon (TOC) content was determined with a TOC analyzer (Germany Multi-N/C 2000).

To find out which reactive species play more significant role in the photodegradation of Rh B, the scavenging study was performed. At the beginning of visible-light irradiation, Sodium oxalate and Cr (VI) with the concentration of 5 mmol/l were added to capture photoinduced holes and electrons [43,44], respectively. Substitution of adsorption hydroxyls on the surface of photocatalyst (OH_{ads}^-) was carried out by adding sodium fluoride (5 mmol/l) in the aqueous nanofibers suspension (100 mg/l), and the F^- surface modified nanofibers were obtained after being filtered and dried [45].

3. Results and discussion

3.1. Characterization of S-doped TiO_2 nanofibers

SEM images of the typical xerogel fibers and annealed TiO_2 nanofibers were shown in Fig. 1. Before thermal treatment, the

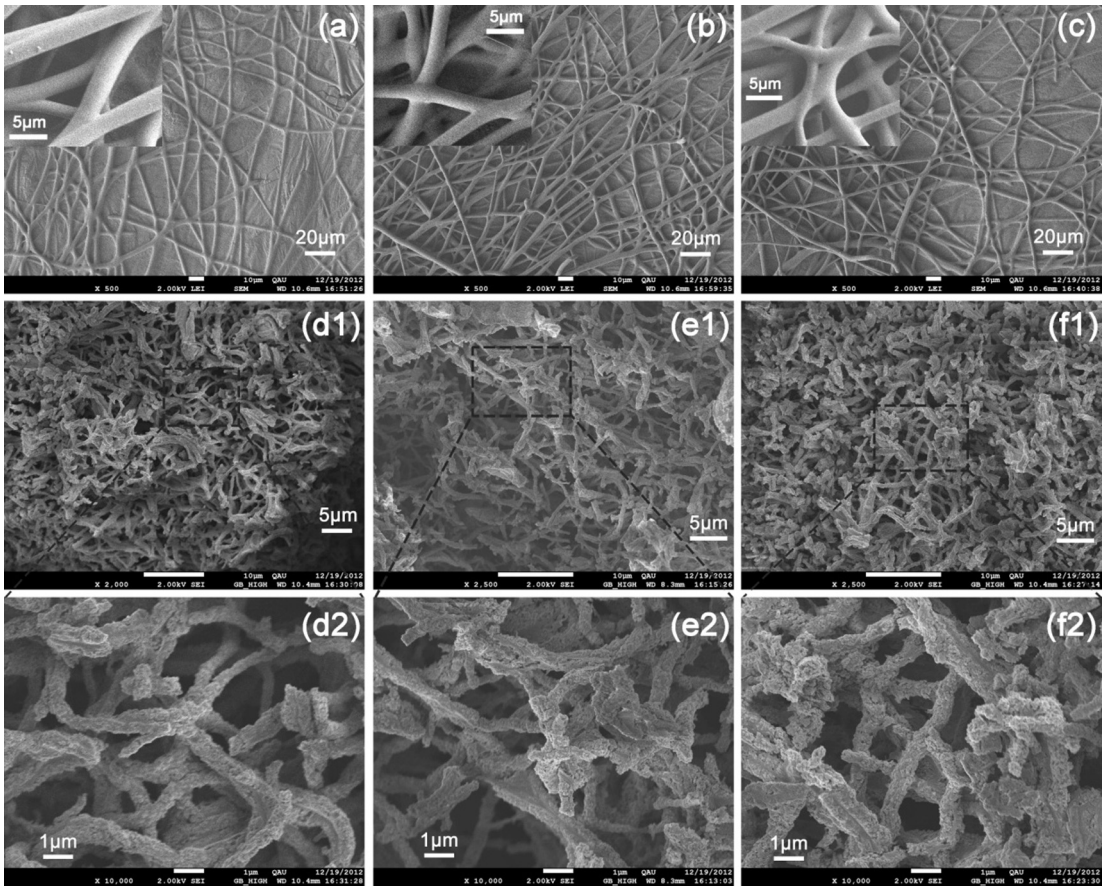

Fig. 1. SEM images of pure and S-doped TiO_2 photocatalysts: (a) TF as-spun; (b) UTF as-spun; (c) CTF as-spun; (d) TF calcined after 500 °C; (e) UTF calcined after 500 °C; (f) CTF calcined after 500 °C.

as-spun fibers appeared a random orientation and a uniform surface over the substrate as shown in Fig. 1(a–c). The fibers were continuous with 5–20 cm in length, and 2–4 μm in diameter. After calcinations at 500 °C, coarser surface was appeared in the fibers, as shown in Fig. 1(d–f). The outer diameters of the catalysts decreased to normally several hundred nanometers, and the fibers became discontinuous as well. The shrinkage of fibers was largely because of the decomposition of PVP and crystallization of TTIP. As a result of sintering, large interconnected holes were generated within the fibers, and a 3D fibrous network was completely formed. These suggested that the S-doping made no obvious change in the morphology of fibrous catalysts.

The EDX microanalysis spectra of the pure and S-doped TiO_2 photocatalysts were shown in Fig. 2(a–c). The spectra revealed that the materials were mainly composed of Ti and O. Signals corresponding to sulfur at about 2.3 keV were clearly distinct in samples of TTF and CTF, which attributed to a small amount of sulfur atoms. But the signals of S were not detected in the pure TiO_2 sample.

The TG curves (Fig. 3) of the as-spun fibers showed three steps and a total weight loss of ca. 84%. The initial weight loss of ca. 11% occurred below 200 °C, which was due to the desorption of solvent. The following significant weight loss of ca. 40% in the range of 300–400 °C was assigned to the decomposition of the side chain of PVP and residual other organic material. Between 400 and 500 °C, there was a weight loss of ca. 33%, which was attributed to the complete decomposition of the main polymer chain of PVP [19]. Above 500 °C, the weight of the samples remained constant, which indicated that the organic component had been entirely decomposed. According to SEM observation, well-defined fiber texture was still retained after calcination at 500 °C, indicating that the removal of

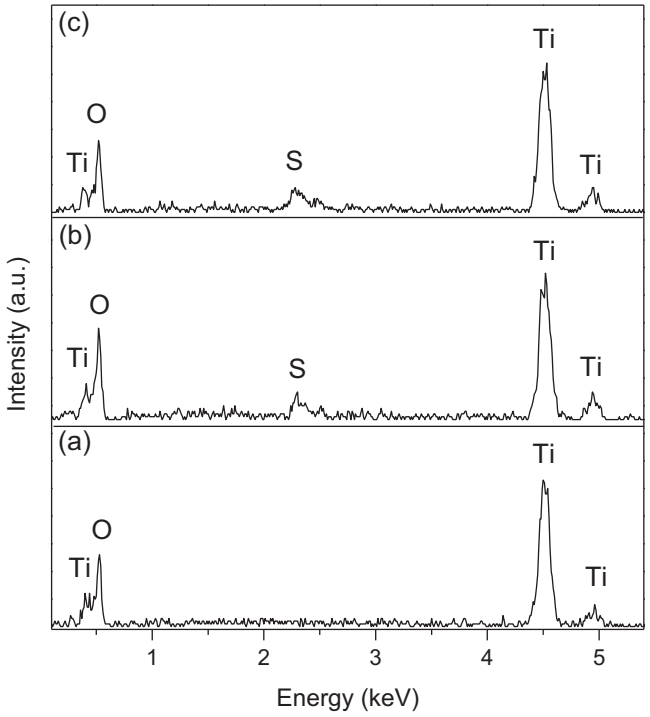

Fig. 2. EDX microanalysis spectra of pure and S-doped TiO_2 photocatalysts calcined after 500 °C: (a) TF; (b) UTF; (c) CTF.

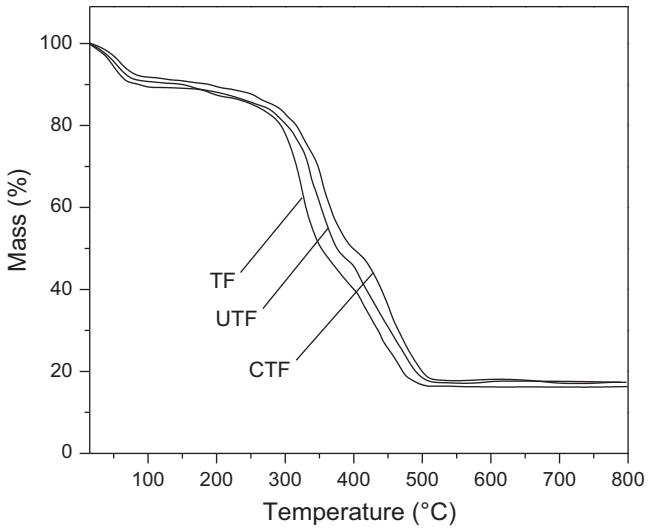

Fig. 3. TG curves of the as-spun TF, UTF, and CTF fibers under air atmosphere.

PVP could not destroy one-dimensional morphology of fibers, and PVP was an excellent adhesive and template in the electrospinning system [7].

As shown in Fig. 4, the XRD patterns for TiO_2 and S-doped TiO_2 nanofibers could be ascribed to a mixed phase of anatase and rutile after calcination at 500 °C. In pure TiO_2 nanofibers, the strong diffraction peak of the (1 1 0) crystal plane demonstrated that the rutile phase made up a considerable proportion of 45.5%. But the diffraction intensity for rutile phase was extremely weak in samples of TTF and CTF, indicating that the S-doping could effectively inhibit the growth of rutile phase. At the same time, it was found that the average crystallite sizes of S-doped samples, determined by the Debye-Scherrer equation, were apparently smaller than that of undoped one (Table 1). It suggested that the anatase crystallization in the catalysts was strongly affected by S-doping.

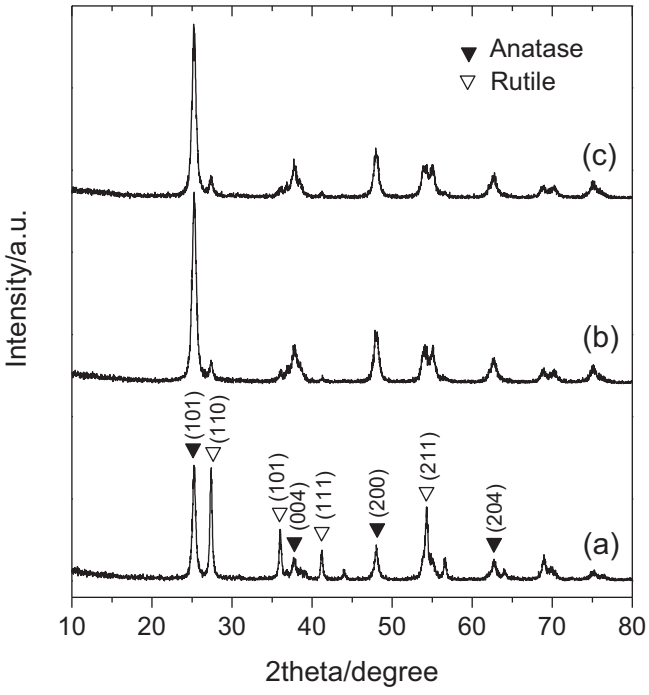

Fig. 4. XRD patterns of pure and S-doped TiO_2 nanofibers after calcined at 500 °C: (a) TF; (b) UTF; (c) CTF.

Furthermore, the unit cell parameters of the Tetragonal crystal system in obtained samples were calculated and listed in Table 1, and it could be observed that the lattice constants were slightly changed after sulfur doping, which was consistent with the former results [41,46].

High-resolution XPS spectra in S 2p, Ti 2p and O 1s region of pure and S-doped TiO_2 nanofibers were shown in Fig. 5. In the spectra of S 2p region, the S atoms were present in both UTF and CTF materials (b and c), but absent in the pure sample (a), revealing sulfur atoms were successfully incorporated into the bulk phase of the doped TiO_2 nanofibers.

The UTF catalyst, employing thiourea as the sulfur precursor, showed only a peak around 169.2 eV (Fig. 5b1), and it should be emphasized that the sulfur atoms were all in the state of S^{6+} in the sample of UTF. It should be mentioned here that before measured by XPS method, the sample of UTF was washed with deionized water several times. This revealed that the sulfur atoms were not in the form of physisorbed species on catalyst surface such as SO_4^{2-}. Previous study [33–36] reported that the substitution of Ti^{4+} by S^{6+} would be achieved when thiourea was used as dopant. Those results were in good coincidence with ours in Fig. 5b2. After Ar^+ sputtering to about 10 nm in deep, the peak around 169.2 eV was remaining. This strongly indicated that the sulfur atoms entered the bulk phase of TiO_2 and substitute for Ti atoms. As we know, the atomic radius of Ti^{4+} (0.64 Å) is relatively larger than that of S^{6+} (0.29 Å). Thus, the cationic S-doped sample with the substitution of Ti^{4+} by S^{6+} might cause the decrease of the crystal size. This inference was in good accordance with the crystal information due to the XRD patterns (Table 1), in which the lattice parameters (*a*, *c*, and *V*) of UTF catalyst were smaller than those of pure one.

The XPS spectra of CTF catalyst (Fig. 5c1) demonstrated that the presence of sulfur species corresponds to the binding energy (BE) around 168.9 eV and 163.6 eV in S 2p level. These two peaks were due to the presence of the highest oxidation states such as SO_4^{2-} and lower valence state of S^{2-}, respectively. However, the peak around 168.9 eV was disappeared after Ar^+ sputtering (Fig. 5c2), and at the same time, the S^{2-} peak remained. Further works [31,32] found that the S-doping was in the anionic form when TiS_2, or CS_2 were used as the sulfur precursors. In our case, the peak around 163.6 eV attributed to the S^{2-} species, corresponding to the anionic S-doping in the bulk TiO_2 with the substitution of O^{2-} by S^{2-}. This suggested that some residual sulfur from CS_2 naturally remained and formed Ti—S bond after the electrospinning and thermal treatment process.

Furthermore, the peak at 168.9 eV in curve c1 ought to be considered as oxidized products derived from S^{2-}. The SO_4^{2-} groups were probably formed between sulfur and oxygen atoms on surface of the CTF catalyst with calcination process. The ion substitution in the bulk TiO_2 would create some change on unit cell parameters, because of the difference in the ionic radius between O^{2-} (1.22 Å) and S^{2-} (1.7 Å). With the substitution of O^{2-} by S^{2-} in CTF catalyst, unit cell parameters (*a*/*b*, *c* and *V*) were found slight increases compared with TF and UTF catalysts (Table 1), just because of the larger ionic radius of S^{2-} than that of O^{2-}, and which is consistent with the XPS results.

The spectra of Ti 2p and O 1s regions based on the pure and S-doped catalysts were shown in Fig. 5 as well. The binding energy of Ti and O in the S-doped catalysts shifted negatively in comparison with that in undoped one. It should be mentioned that the cationic and anionic S-doping resulted in the formation of Ti—O—S and O—Ti—S bands in the lattice, respectively. Due to the higher electronegativity of the titanium and the oxygen atoms, partial electrons transferred from the sulfur atom to them, and a charge imbalance was accordingly created and a new band energy structure formed [46,47]. The end result was the peak shifting to the lower binding energy.

Table 1
Sulfur content, crystal size, and photocatalytic properties of TF, UTF, and CTF samples.

Sample	Sulfur content (at%)[a]	Anatase phase (%)	D (nm)	Unit cell parameters			Band gap (eV)	Photodegraded of Rh B (%)[b]
				a/b (Å)	c (Å)	V (nm^3)		
TF	–	45.8	20.8	3.7847	9.6959	0.1389	3.11	15
UTF	0.84	87.6	12.8	3.7788	9.6247	0.1374	2.86	83
CTF	1.26	86.8	13.8	3.7907	9.7105	0.1395	2.81	89

[a] Measured by XPS.
[b] Measured after 120 min in visible-light irradiation.

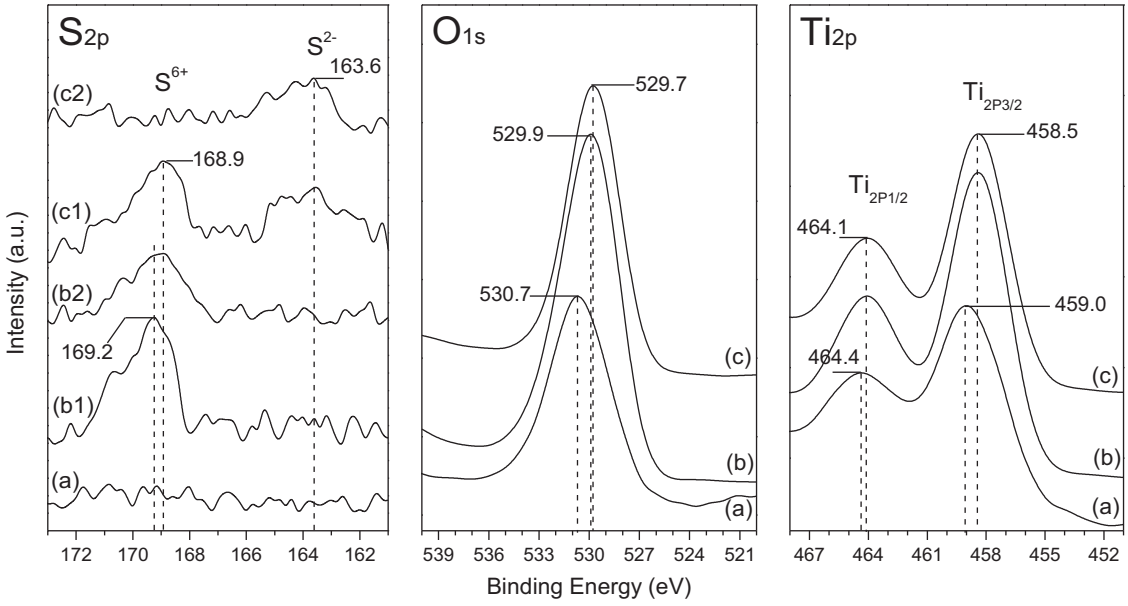

Fig. 5. High-resolution XPS spectra of S 2p, Ti 2p and O 1s of pure TiO_2 (a), S-doped TiO_2 nanofibers of UTF (b), and CTF (c). The spectra denoted as (b1) and (c1): before Ar^+ sputtering; (b2) and (c2): after Ar^+ sputtering (0.1 nm/min) to a depth of 10 nm for 15 min.

The FT-IR spectra of pure TiO_2 (TF) and S-doped TiO_2 (UTF and CTF) nanofibers calcined at 500 °C were shown in Fig. 6. The broad intense band in the range of 800–400 cm^{-1} could be attributed to the stretching vibration of Ti—O—Ti. The peaks around 1090, and 1411 cm^{-1} were due to the characteristic frequencies of SO_4^{2-} bidentate bond [48], and the peak around 1337 cm^{-1} was due to the he stretching frequency of S=O [49]. These peaks were present in both UTF and CTF samples, indicated that the bidentate SO_4^{2-} coordinated to the surface of the S-doped TiO_2 nanofibers. The other absorbance band at 1048 cm^{-1}, appearing only in CTF sample, indicated a Ti—S stretching vibration [39], suggesting the successful anionic doping of sulfur atom with the substitution of O^{2-} by S^{2-}. The results were in well accordance with the XPS results, since the peak of S^{2-} was present in CTF sample. The FT-IR bands related to S—O/S=O and Ti—S bonds were not found in the pure TiO_2 sample (TF), which suggested that the doping did not arise from any impurities present in the precursors, but occurred as a result of the electrospinning doping process. The peaks around 1630 cm^{-1} corresponded to the bending vibrations of the O—H bond, and in comparison with the TF and CTF, the intensity of the peak in UTF sample was much stronger. This indicated that the introduction of cationic S-doping could make more hydroxyl groups on the UTF surface, which played a vital role in photodegradation of organic pollutants.

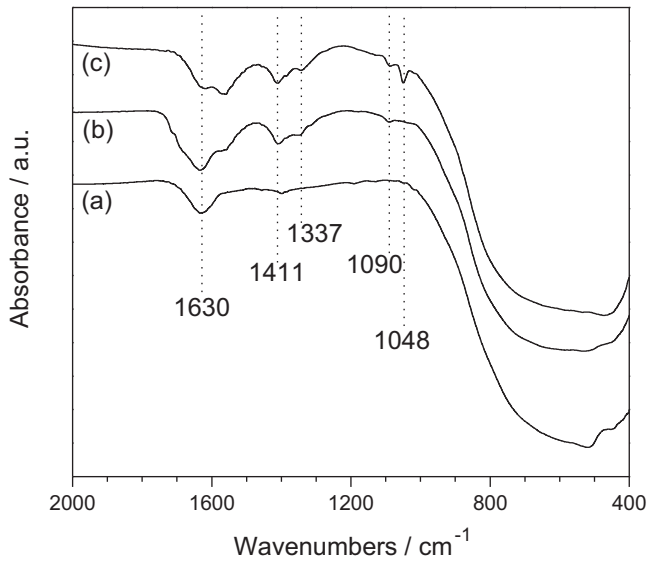

Fig. 6. FTIR spectra of (a) TF, (b) UTF, and (c) CTF samples calcined at 500 °C.

According to EDX, XRD, XPS and FT-IR results in the present work, the possible structure of S-doped TiO_2 nanofibers (UTF and CTF) was inferred and shown in Scheme 1. It could be tentatively concluded that the S-doped TiO_2 nanofibers showed cationic (UTF) and anionic (CTF) formation corresponding to the sulfur precursor with thiourea and CS_2 separately, that is, sulfur precursor played a significant role in valence state of sulfur in doped nanofibers. In the UTF sample, on the one hand, we concluded that the S^{6+} substituted for Ti^{4+} cation and a Ti—O—S bond was performed, and the formation of a charge imbalance between sulfur and oxygen atoms eventually created hydroxide to neutralize the extra positive charge. In addition, some SO_4^{2-} groups were appeared on the surface of the catalyst by chemisorptions. On the other hand, the

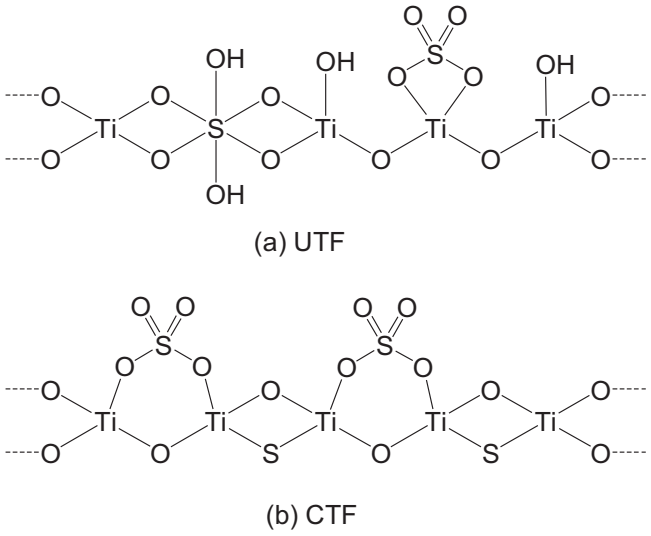

Scheme 1. Possible structure of cationic and anionic S-doped TiO_2 nanofibers.

S-doping in the CTF samples demonstrated that the O—Ti—S was present, in which the O atom in the O—Ti—O network was partly replaced by the S atom. It should be noted that although the valence state of S^{2-} was mainly present in the lattice of CTF samples, oxidation state of sulfur, such as SO_4^{2-}, also chemisorbed on its surface due to the calcination process.

The UV–vis diffuse reflectance spectra of pure TiO_2 (TF) and S-doped TiO_2 nanofibers (UTF and CTF) were shown in Fig. 7. The S-doping catalysts exhibited stronger light absorbance in visible region. According to the equation of $Ah\nu = K(h\nu - E_g)^2$, a plot of $(Ah\nu)^{0.5}$ vs. $h\nu$ based on the direct transition was shown in Fig. 7 (inset). The extraploted vaule of $h\nu$ at $A = 0$ revealed a absorption edge energy. The pure TiO_2 catalyst displayed no significant light absorbance in visible region due to its large bang gap of 3.11 eV. After loading of sulfur atoms into TiO_2 nanofibers, the photoabsorption on visible region obviously increased, and the band-gap energy for samples of UTF and CTF were down to about 2.86 and 2.81 eV, respectively. Undoubtedly, these results suggested that the sulfur atoms were indeed doped into the bulk TiO_2, and the alteration of crystal and electronic structures of doped materials resulted in

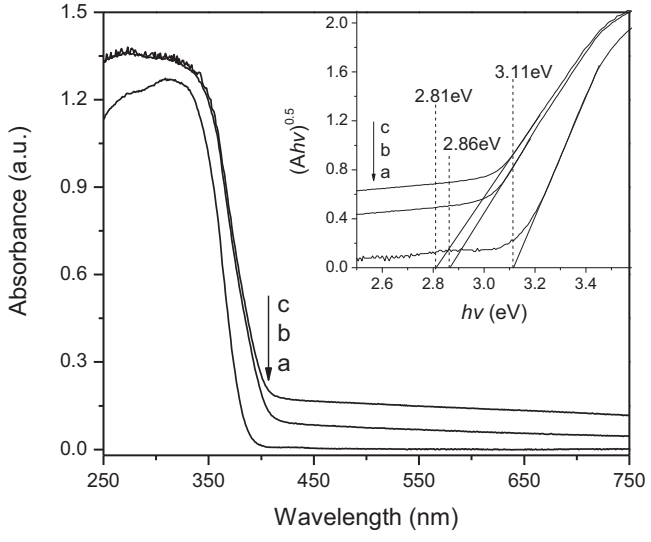

Fig. 7. UV–vis DRS spectra of (a) TF, (b) UTF, and (c) CTF samples calcined at 500 °C. Inset: $(Ah\nu)^{0.5}$ vs. $h\nu$ for the pure and S-doped nanofibers, extrapolating the linear part gives direct values of band gap.

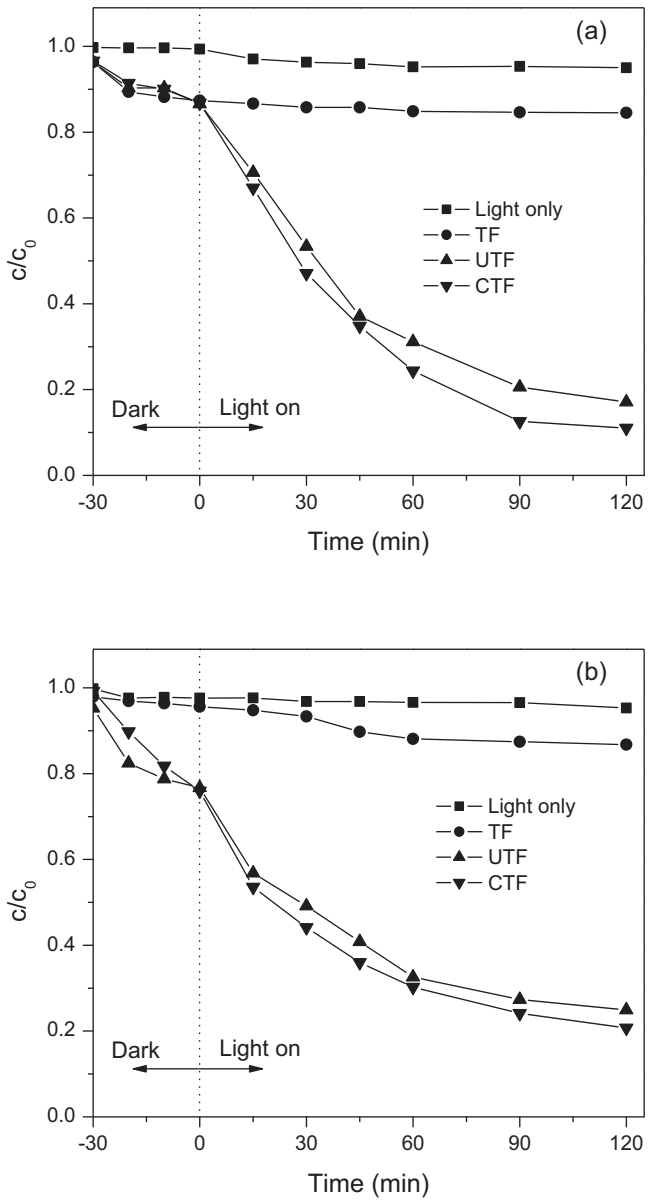

Fig. 8. Plots of photodegradation of Rh B (a) and phenol (b) under visible-light irradiation with 0.25 g catalyst per 250 ml solution.

the stronger absorption in visible-light area. Comparison with TF, a broad background absorption in the visible light region more than 500 nm was observed in both UTF and CTF samples. The enhanced light absorption was attributed to the formation of Ti—O—S or O—Ti—S bonds, which could lead partial electrons to transfer from the sulfur atom to Ti and O atoms. Then the low-valence state was appeared [50], and it would show a wide and strong absorption in the wavelength range more than 500 nm, which is consistent with the XPS results. A similar effect was reported in carbon modified TiO_2 composites [51].

3.2. Photocatalytic activity and mechanism

To compare the photocatalytic activity of the pure and S-doped TiO_2 nanofibers, the reaction of Rh B degradation in an aqueous solution was performed as photoreaction probes in visible-light irradiation ($\lambda \geq 420$ nm), which was shown in Fig. 8(a). In the visible-light irradiation without photocatalyst, the dye decreased weakly after 120 min, indicating no photolysis of Rh B in visible

irradiation alone. The photodegradation plot of the pure TiO_2 (TF) showed just dark adsorption, suggesting that the catalyst had no response to visible-light. However, the S-doped TiO_2 nanofibers revealed higher visible photocatalytic activity than the pure one, with the UTF and CTF samples showing the Rh B conversions of 83% and 89% after 120 min irradiation, respectively.

In order to avoid photosensitization effect, phenol was selected as substrate to evaluate the photocatalytic activity of the nanofibers because it would not absorb in visible region. As shown in Fig. 8(b), it was found that more than 75% of phenol was degraded in 120 min by using UTF or CTF photocatalyst, and the removal rate was similar to the Rh B photodegradation. The results indicated that the organic compounds (Rh B or phenol) would not undergo degradation on photocatalysts surface under visible light by sensitization process. The photodegradation mechanism of S-doped TiO_2 nanofibers presented in this work should involve photoinduced charge separation in photocatalysts as a result of bandgap excitation.

In order to find which reactive species played more significant role in the photodegradation of Rh B by S-doped TiO_2 nanofibers, the scavenging experiments were performed. Different scavengers were employed individually to remove the specific reactive species. F^- surface substitution was used to remove the OH_{ads^-} because fluoride showed stronger adsorption on catalyst surface [43], which resulted in the minimization of the surface OH_{ads^-}, then the remarkable increase of $^{\bullet}OH$ radicals.

In Fig. 9(a), substitution of OH_{ads^-} by F^- on UTF surface made an obvious decrease of Rh B conversion, indicating the OH_{ads^-} is important for the photocatalytic process of the UTF sample. Meanwhile, the photodegradation efficiency is significantly decreased by adding sodium oxalate as h^+ scavenger, showing the h^+ played a leading part in the OH^- induced reaction. In addition, it was found that photodegradation efficiency was a bit increase after adding Cr(VI) as e^- scavenger, indicating e^- located in the CB was unvalued species in Rh B conversion by UTF sample. Furthermore, scavenging e^- could inhibit its recombination with the photo-induced h^+, which could probably help to enhance the reaction rate slightly.

Fig. 9(b) showed the plots of Rh B photodegradation by CTF sample. No distinct change was found in photoreaction process by adding scavenger of $OH_{ads}{}^-$, which was probably due to the absence of $OH_{ads}{}^-$ on CTF surface. The photodegradation efficiency was decreased from 89% to 58% after adding h^+ scavenger, and it is supposed that the photoinduced h^+ could be the primary reactive species for the visible-light induced reaction by CTF photocatalyst. However, it should be noted that photoinduced e^- played an important role in Rh B photodegradation when h^+ was scavenged. Moreover, scavenging electrons could inhibit the recombination of the photo-induced h^+ and e^-, thus the similar result was found in CTF as UTF sample.

The above results suggested that cationic and anionic S-doping with TiO_2 nanofibers had fundamentally different mechanism in photodegradation reaction. Scheme 2 displayed the possible mechanism for both systems.

In the UTF system, cationic S-doped TiO_2 nanofibers were formed when thiourea was used as the sulfur precursors. The substitution of Ti^{4+} by S^{6+} would be similar to the situation of transition-metal ion doping [52], and intra-band-gap states close to the CB edges were created to induce visible-light absorption. On the other hand, it should be created a charge imbalance in the bulk of TiO_2 when the S^{6+} ions replace the Ti^{4+} ions, and considerable anions such as hydroxyl ions could be adsorbed to neutralize the extra positive charge [34]. Thus, the exhibited higher activity of UTF sample could be explained by the following factors: (i) the substitution of Ti^{4+} by S^{6+} in the TiO_2 lattice might lead to the generation of localized sulfur midgap levels located under the Ti 3d CB, and the new impurity level had narrower band gap than pure TiO_2 and could increase the absorption in the visible-light region. (ii) More

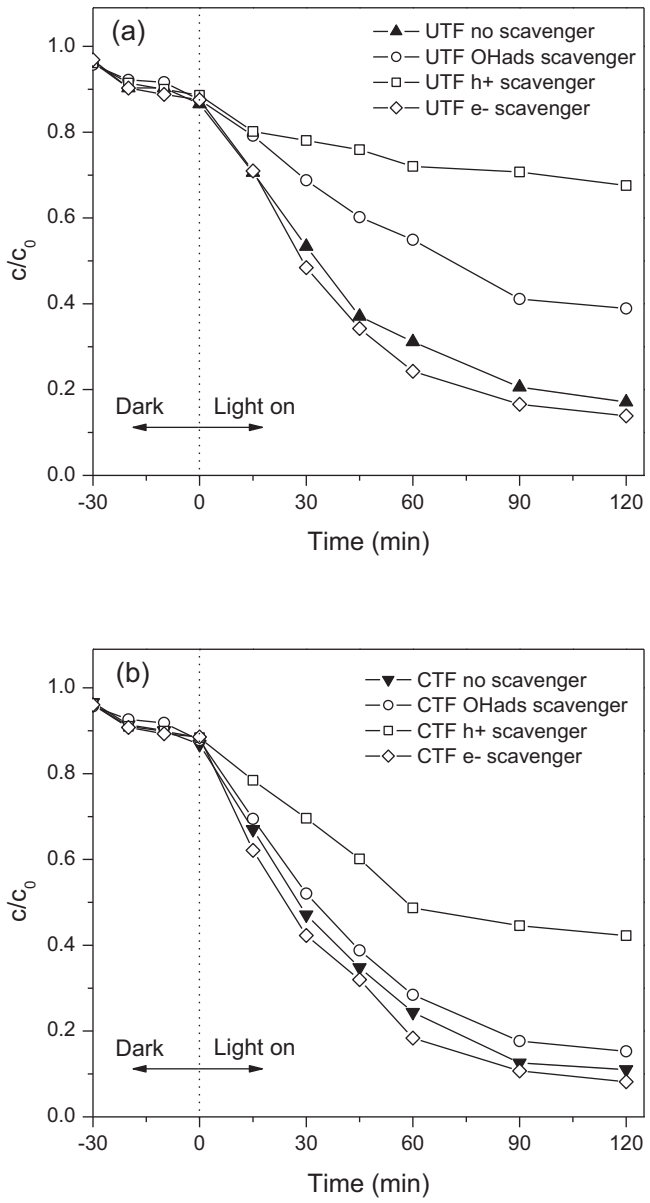

Fig. 9. Plots of photodegradation of Rh B in the presence of UTF (a) and CTF (b) with different scavengers. Scavengers were employed with the following reagents: 5 mmol/l sodium fluoride for OH_{ads^-} by F^- surface modification before photoreaction; 0.5 mmol/L sodium oxalate for h^+, and 0.05 mmol/l Cr(VI) for e^-.

importantly, plenty of hydroxyl ions were adsorbed on the surface of the TiO_2 lattice, and they could capture the photoinduced h^+ to form active groups typically as hydroxyl radical, that was the main species responsible for the degradation of organic pollutants. (iii) According to the results from the procedure of h^+ scavenging, the photoinduced h^+ played an important role to produce hydroxyl radical by means of hydroxyl ions oxidation in solution. (iv) With the formation of Ti—O—S bond, partial e^- transferred from sulfur to oxygen atoms, and the electron-deficient sulfur atoms might capture the e^- and then inhibited the recombination between the h^+ and e^-, resulting in high quantum efficiency.

In the CTF system, CS_2 was employed as the sulfur precursors and anionic S-doped TiO_2 nanofibers were generated. Base on the DRS spectra and photocatalytic process of Rh B, CTF system had narrower band gap and higher photodegradation efficiency than TF and UTF systems. It could have the following reasons: (i) the formation of O—Ti—S and Ti—O—S in the crystal structure of TiO_2

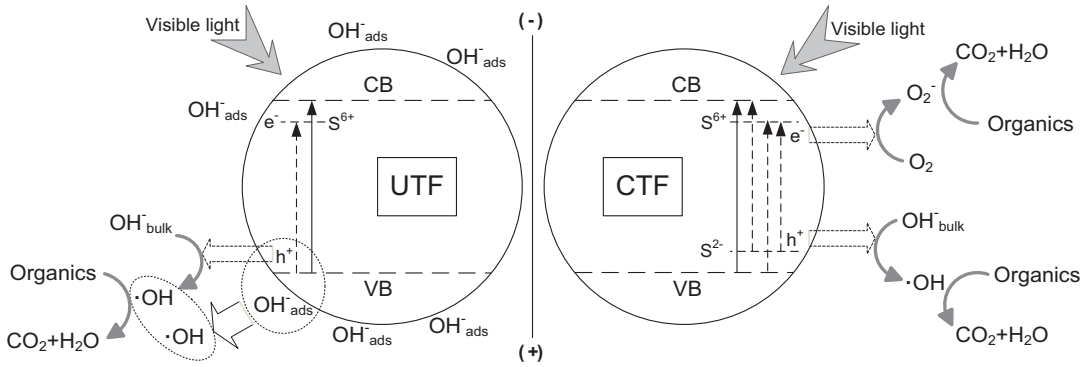

Scheme 2. Possible photodegradation mechanism of S-doped TiO_2 nanofibers in visible-light irradiation.

could introduce several new impurity levels between the CB and VB, thus much more photoinduced e^- transferred to the CB in visible-light irradiation, then the photoinduced h^+ could be promote to produce more active radicals. (ii) S-doping modified the lattice structure of TiO_2, and generated more oxygen vacancies and defects, which were important for absorption in visible-light and even more important to capture the photoinduced e^- to inhibit the recombination of the h^+ and e^-, thus to improve the quantum efficiency. (iii) According to the results from photodegradation process, not only h^+ but e^- migrated to the surface of photocatalysts, combined with the adsorbed H_2O and O_2, and produced hydroxyl and superoxide radicals, respectively, then initiated the degradation of Rh B.

3.3. Mineralization ability and stability

In order to evaluate the complete degradation of organic compounds on the photocatalysis process, TOC concentration as a function of irradiation time was usually analyzed [53–55]. Significant mineralization of Rh B dye and phenol was observed (Fig. 10a and b) in present work, and the TOC removal of Rh B and phenol was up to 50% and 46% in 120 min visible light irradiation, respectively. This indicated that the photodegradation with as-prepared S-doped TiO_2 nanofibers was not only a bleaching or a decomposing, but also a deep oxidation process to mineralize organic molecules into inorganic ones, such as CO_2 and H_2O.

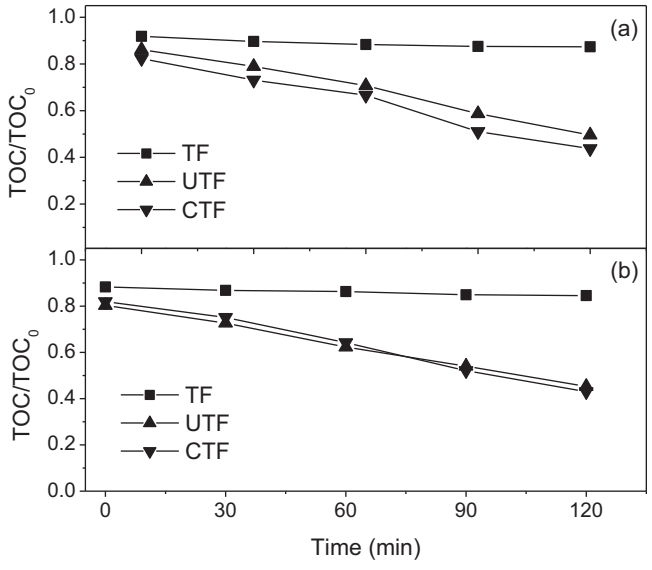

Fig. 10. The TOC/TOC_0 vs. reaction time for mineralization of Rh B (a) and phenol (b) in the presence of TF, UTF and CTF under visible-light irradiation.

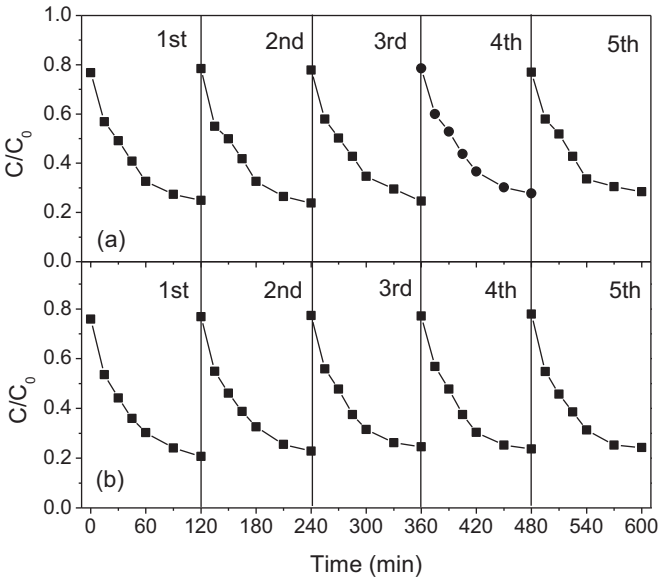

Fig. 11. Cycling runs in photodegradation of Rh B in the presence of UTF (a) and CTF (b) under visible-light irradiation.

To evaluate the stability of the S-doped TiO_2 nanofibers, repeated experiments of degredation of Rh B were carried out. As shown in Fig. 11a and b, the UTF and CTF samples exhibited almost no changes in photocatalytic activity during five cycles of the photodegradation, indicating that the as-prepared nanofibers was photocatalytically stable and did not suffer from photocorrosion.

4. Conclusion

In summary, we successfully developed cationic and anionic S-doped TiO_2 nanofibers by electrospinning method employing thiourea and CS_2 as the sulfur precursors, respectively. The S-doped TiO_2 nanofibers showed significant photodegradation and mineralization of organic compounds compared with undoped one. In cationic S-doped sample, the crystalline grain reduced in size via S^{6+} substituted for Ti^{4+}, because S^{6+} had a significantly smaller ionic radius compared to that of Ti^{4+}. Similarly, the crystalline grain increased when O^{2-} was substituted by S^{2-} in anionic S-doped sample. These substitutions made the lower BE shifting of titanium and oxygen peaks because of their higher electronegativity, and ultimately resulted in the stronger light absorbance in visible region. The SO_4^{2-} groups were appeared on the surface of both cationic and anionic S-doped TiO_2 nanofibers, revealing the oxidation of surface sulfur atoms and further chemisorptions. The cationic S-doped TiO_2 nanofibers exhibited higher photocatalytic

activity, mainly because of the formation of the new impurity level and the much more chemisorbed hydroxyl ions on the sample surface, which could be oxidized by the photoinduced holes. In the anionic S-doped system, however, holes and electrons had the nearly equal importance function, and its higher photocatalytic activity mainly because of the higher quantum efficiency. Ultimately, we suggested that the photocatalytic activity of the S-doped TiO_2 nanofibers depend of the doping species and the chemisorbed hydroxylation degree on the surface.

Acknowledgments

This work was supported by National Natural Science Foundation of China (nos. 20907025, 51208274), Natural Science Foundation of Shandong province (no. ZR2012EEQ010), and Key Program of Qingdao Agricultural University (no. 6610903).

References

[1] J. Doshi, D.H. Reneker, J. Electrostat. 35 (1995) 151–160.
[2] Y. Dzenis, Science 304 (2004) 1917–1919.
[3] S.N. Jayasinghe, A.C. Sullivan, J. Phys. Chem. B 110 (2006) 2522–2528.
[4] S. Madhugiri, A. Dalton, J. Gutierrez, J.P. Ferraris, K.J. Balkus, J. Am. Chem. Soc. 125 (2003) 14531–14538.
[5] J. Yu, S.V. Fridrikh, G.C. Rutledge, Adv. Mater. 16 (2004) 1562–1566.
[6] W. Li, S. Zhao, B. Qi, Y. Du, X. Wang, M. Huo, Appl. Catal. B Environ. 92 (2009) 333–340.
[7] G. Zhao, S. Liu, Q. Lu, L. Song, Ind. Eng. Chem. Res. 51 (2012) 10307–10312.
[8] D. Li, Y. Xia, Nano Lett. 3 (2003) 555–560.
[9] S. Zhan, D. Chen, X. Jiao, C. Tao, J. Phys. Chem. B 110 (2006) 11199–11204.
[10] S. Chuangchote, J. Jitputti, T. Sagawa, S. Yoshikawa, ACS Appl. Mater. Interfaces 1 (2009) 1140–1143.
[11] C. Li, G. Xu, B. Zhang, J. Gong, Appl. Catal. B Environ. 115–116 (2012) 201–208.
[12] X. Li, F. Li, Environ. Sci. Technol. 35 (2001) 2381–2387.
[13] G. Li, D. Zhang, J.C. Yu, Environ. Sci. Technol. 43 (2009) 7079–7085.
[14] R. Asahi, T. Morikawa, T. Ohwaki, K. Aoki, Y. Taga, Science 293 (2001) 269–271.
[15] M. Jin, X. Zhang, S. Nishimoto, Z. Liu, D.A. Tryk, A.V. Emeline, T. Murakami, A. Fujishima, J. Phys. Chem. C 111 (2007) 658–665.
[16] Z. Liu, D.D. Sun, P. Guo, J.O. Leckie, Nano Lett. 7 (2007) 1081–1085.
[17] Y. Yang, H. Wang, X. Li, C. Wang, Mater. Lett. 63 (2009) 331–333.
[18] D.Y. Lee, B. Kim, N. Cho, Y. Oh, Curr. Appl. Phys. 11 (2011) S324–S327.
[19] I. Cacciotti, A. Bianco, G. Pezzotti, G. Gusmano, Chem. Eng. J. 166 (2011) 751–764.
[20] J. Kaewsaenee, P. Visal-athaphand, P. Supaphol, V. Pavarajarn, Ind. Eng. Chem. Res. 50 (2011) 8042–8049.
[21] J. Park, J. Lee, D. Choi, C. Hwang, J. Lee, Mater. Lett. 88 (2012) 156–159.
[22] A.L. Linsebigler, G. Lu, J.T. Yates Jr., Chem. Rev. 95 (1995) 735–758.
[23] X. Chen, S.S. Mao, Chem. Rev. 107 (2007) 2891–2959.
[24] V.C. Di, G. Pacchioni, A. Selloni, S. Livraghi, E. Giamello, J. Phys. Chem. B 109 (2005) 11414–11419.
[25] F. Dong, Z. Wu, S. Guo, J. Hazard. Mater. 162 (2009) 763–770.
[26] D. Teng, Y. Yu, H. Liu, X. Yang, S. Ryu, Y. Lin, Catal. Commun. 10 (2009) 442–446.
[27] J.B. Veluru, S.N. Appukuttan, P. Zhu, R. Seeram, Mater. Lett. 65 (2011) 3064–3068.
[28] D.D. Camillo, F. Ruggieri, S. Santucci, L. Lozzi, J. Phys. Chem. C 116 (2012) 18427–18431.
[29] T. Umebayashi, T. Yamaki, H. Itoh, K. Asai, Appl. Phys. Lett. 81 (2002) 454–456.
[30] T. Umebayashi, T. Yamaki, S. Yamamoto, A. Miyashita, S. Tanaka, T. Sumita, K. Asai, J. Appl. Phys. 93 (2003) 5156–5160.
[31] W. Ho, J.C. Yu, S. Lee, J. Solid State Chem. 179 (2006) 1171–1176.
[32] H. Li, X. Zhang, Y. Huo, J. Zhu, Environ. Sci. Technol. 41 (2007) 4410–4414.
[33] T. Ohno, T. Mitsui, M. Matsumura, Chem. Lett. 32 (2003) 364–365.
[34] J.C. Yu, W. Ho, J. Yu, H. Yip, P.K. Wong, J. Zhao, Environ. Sci. Technol. 39 (2005) 1175–1179.
[35] J. Xu, J. Li, W. Dai, Y. Cao, H. Li, K. Fan, Appl. Catal. B Environ. 79 (2008) 72–80.
[36] T. Sano, N. Mera, Y. Kanai, C. Nishimoto, S. Tsutsui, T. Hirakawa, N. Negishi, Appl. Catal. B Environ. 128 (2012) 77–83.
[37] T. Ohno, M. Akiyoshi, T. Umebayashi, K. Asai, T. Mitsui, M. Matsumura, Appl. Catal. A Gen. 265 (2004) 115–121.
[38] J.A. Rengifo-Herrera, J. Kiwi, C. Pulgarin, J. Photochem. Photobiol. A Chem. 205 (2009) 109–115.
[39] G. Yang, Z. Jiang, H. Shi, M.O. Jones, T. Xiao, P.P. Edwards, Z. Yan, Appl. Catal. B Environ. 96 (2010) 458–465.
[40] G. Yan, M. Zhang, J. Hou, J. Yang, Mater. Chem. Phys. 129 (2011) 553–557.
[41] S. Liu, Q. Tang, Q. Feng, Appl. Surf. Sci. 257 (2011) 5544–5551.
[42] R.A. Spurr, H. Myers, Anal. Chem. 29 (1957) 760–762.
[43] P. Calza, E. Pelizzetti, Pure Appl. Chem. 73 (2001) 1839–1848.
[44] R. Jin, W. Gao, J. Chen, H. Zeng, F. Zhang, Z. Liu, N. Guan, J. Photochem. Photobiol. A Chem. 162 (2004) 585–590.
[45] Y. Chen, S. Yang, K. Wang, L. Lou, J. Photochem. Photobiol. A Chem. 172 (2005) 47–54.
[46] H. Znad, Y. Kawase, J. Mol. Catal. A Chem. 314 (2009) 55–62.
[47] J.A. Rengifo-Herrera, E. Mielczarski, J. Mielczarski, N.C. Castillo, J. Kiwi, C. Pulgarin, Appl. Catal. B Environ. 84 (2008) 448–456.
[48] X. Wang, J.C. Yu, P. Liu, X. Wang, W. Su, X. Fu, J. Photochem. Photobiol. A Chem. 179 (2006) 339–347.
[49] K.M. Parida, N. Sahu, N.R. Biswal, B. Naik, A.C. Pradhan, J. Colloid Interface Sci. 318 (2008) 231–237.
[50] S. Yin, K. Ihara, Y. Aita, M. Komatsu, T. Sato, J. Photochem. Photobiol. A Chem. 179 (2006) 105–114.
[51] H. Zhang, X. Lv, Y. Li, Y. Wang, J. Li, ACS Nano 4 (2010) 380–386.
[52] H. Kisch, W. Macyk, ChemPhysChem 3 (2002) 399–400.
[53] A. Durán, J.M. Monteagudo, I. Sanmartín, A. García-Díaz, Appl. Catal. B Environ. 138–139 (2013) 318–325.
[54] E. Brillas, J. Calpe, P. Cabot, Appl. Catal. B Environ. 46 (2003) 381–391.
[55] C. Wang, L. Zhu, C. Song, G. Shan, P. Chen, Appl. Catal. B Environ. 105 (2011) 229–236.